Earth and Planetary Science Letters 362 (2013) 151–162

Contents lists available at SciVerse ScienceDirect

Earth and Planetary Science Letters

journal homepage: www.elsevier.com/locate/epsl

Holocene changes in eastern equatorial Atlantic salinity as estimated by water isotopologues

Guillaume Leduc [a,*], Julian P. Sachs [b], Orest E. Kawka [b], Ralph R. Schneider [a]

[a] Institute of Geosciences, University of Kiel, Ludewig-Meyn-Str. 10, D-24118 Kiel, Germany
[b] University of Washington, School of Oceanography, Box 355351, Seattle, WA 98195, USA

ARTICLE INFO

Article history:
Received 31 January 2012
Received in revised form
8 November 2012
Accepted 1 December 2012
Editor: J. Lynch-Stieglitz

Keywords:
water isotopologues
salinity
eastern equatorial Atlantic
alkenone δD
African monsoon
Holocene

ABSTRACT

The isotopic composition of surface seawater is widely used to infer past changes in sea surface salinity using paired foraminiferal Mg/Ca and $\delta^{18}O$ from marine sediments. At low latitudes, paleosalinity reconstructions using this method have largely been used to document changes in the hydrological cycle. This method usually assumes that the modern seawater $\delta^{18}O$ ($\delta^{18}O_{sw}$)/salinity relationship remained constant through time. Modelling studies have shown that such assumptions may not be valid because large-scale atmospheric circulation patterns linked to global climate changes can alter the seawater $\delta^{18}O_{sw}$/salinity relationship locally. Such processes have not been evidenced by paleo-data so far because there is presently no way to reconstruct past changes in the seawater $\delta^{18}O_{sw}$/salinity relationship. We have addressed this issue by applying a multi-proxy salinity reconstruction from a marine sediment core collected in the Gulf of Guinea. We measured hydrogen isotopes in $C_{37:2}$ alkenones (δD_a) to estimate changes in seawater δD. We find a smooth, long-term increase of ~10‰ in δD_a between 10 and 3 kyr BP, followed by a rapid decrease of ~10‰ in δD_a between 3 kyr BP and core top to values slightly lighter than during the early Holocene. Those features are inconsistent with published salinity estimations based on $\delta^{18}O_{sw}$ and foraminiferal Ba/Ca, as well as nearby continental rainfall history derived from pollen analysis. We combined δD_a and $\delta^{18}O_{sw}$ values to reconstruct a Holocene record of salinity and compared it to a Ba/Ca-derived salinity record from the same sedimentary sequence. This combined method provides salinity trends that are in better agreement with both the Ba/Ca-derived salinity and the regional precipitation changes as inferred from pollen records. Our results illustrate that changes in atmospheric circulation can trigger changes in precipitation isotopes in a counter-intuitive manner that ultimately impacts surface salinity estimates based on seawater isotopic values. Our data suggest that the trends in Holocene rainfall isotopic values at low latitudes may not uniquely result from changes in local precipitation associated with the amount effect.
© 2012 Elsevier B.V. All rights reserved.

1. Introduction

Evidence of past changes in precipitation rates at low latitudes is based on a large array of diverse paleoclimatic proxies. Continental records such as lake sediments commonly use fossil assemblages of diatoms (Gasse, 2002), phytoliths (Alexandre et al., 1998) or pollen (Vincens et al., 2010) to infer past environmental changes linked to the evolution of the hydrological cycle. Paleoprecipitation changes inferred from those proxies depend upon the observed shifts in ecological and environmental conditions induced by climate changes occurring at the regional scale. Another method to derive past rainfall changes over continents relies on the rainwater isotopic signature which is, at low latitudes, inversely related to precipitation rates (Dansgaard, 1964; Rozanski et al., 1993). The $\delta^{18}O$ of rainfall ($\delta^{18}O_r$) fossilized in tropical speleothems has been widely used to reconstruct changes in paleoprecipitation (see e.g. Dykoski et al., 2005; Wang et al., 2005; Fleitmann et al., 2007), even though alterations in large-scale moisture transport can impact the $\delta^{18}O_r$ values locally acquired during precipitation (LeGrande and Schmidt, 2009; Dayem et al., 2010).

In the ocean, sea surface salinity (SSS) is sensitive to evaporation and precipitation occurring at the regional scale, and can be particularly low at low latitudes where precipitation is greater than evaporation and in the vicinity of large river mouths. There is a linear relationship between the isotopic composition of surface seawater (e.g. $\delta^{18}O$ of seawater, $\delta^{18}O_{sw}$) and salinity, which, at low latitudes, is inversely related to precipitation amount (LeGrande and Schmidt, 2006). Reconstructions of past SSS based on $\delta^{18}O_{sw}$ have widely been applied in paleoceanography and use

* Corresponding author.
E-mail address: gl@gpi.uni-kiel.de (G. Leduc).

0012-821X/$ - see front matter © 2012 Elsevier B.V. All rights reserved.
http://dx.doi.org/10.1016/j.epsl.2012.12.003

the modern-day relationship between salinity and $\delta^{18}O_{sw}$ to infer past changes in the hydrological cycle at low latitudes (Schmidt, 1999; Leduc et al., 2009). However, these relationships are based on modern hydrological features, so that any change in the regional hydrological characteristics would cause changes in the $\delta^{18}O_{sw}$/SSS relationship and affect the salinity estimation (Schmidt et al., 2007; LeGrande and Schmidt, 2011).

Hydrogen isotopic measurements performed on C_{37} alkenones contained in marine sediments have recently been applied to reconstruct Late Pleistocene and Holocene hydrological changes in the eastern equatorial Pacific (Pahnke et al., 2007), as well as in the Mediterranean Sea (Van der Meer et al., 2007) and the Black Sea (Van der Meer et al., 2008). As seawater hydrogen isotopes (δD_{sw}) are affected by fractionation processes analogous to those affecting $\delta^{18}O_{sw}$, changes in the δD_{sw}/SSS relationship are also expected to be affected by changes in the hydrological cycle. It has recently been proposed that this issue can be circumvented by combining independent estimates of $\delta^{18}O_{sw}$ and δD_{sw}, to reconstruct past changes in SSS (Rohling, 2007). The combination of both $\delta^{18}O_{sw}$ and δD_{sw} can be jointly used to quantitatively estimate freshwater fluxes that cause salinity changes (Rohling, 2007).

In this study we have measured Holocene changes in hydrogen isotopes in $C_{37:2}$ alkenones (δD_a) extracted from a marine sediment core collected in the Gulf of Guinea (Fig. 1, Weldeab et al., 2007a). This oceanic region has undergone extreme changes in salinity during the Holocene in association with changes in the hydrological cycle occurring in northern Africa (Weldeab et al., 2007b), making the site particularly suitable to apply δD_a. Changes in δD_a values mainly reflect changes in both δD_{sw} (Englebrechts and Sachs, 2003) and salinity (see e.g. Schouten et al., 2006). Comparison of these δD_a data with other salinity proxies is used to identify potential biases embedded in salinity reconstructions from the same core, thereby minimizing uncertainties associated with core chronologies and local oceanographic or depositional effects. We report evidence for past changes in the relationship between seawater stable isotope ratios and salinity that can hamper accurate estimation of rainfall-induced salinity changes based on $\delta^{18}O_{sw}$ and/or δD_{sw} reconstructions.

2. Background on Holocene paleoclimatology in tropical Africa

Evidence suggests that the evolution of Northern tropical African precipitation during the Holocene was triggered by insolation changes, but the timing and trends of paleo-records sensitive to precipitation differ substantially between proxies and locations. Records of vegetation changes (Kröpelin et al., 2008) and of Nile River flood history (Marriner et al., 2012) indicate that a gradual decrease in precipitation occurred in the eastern Sahara during the Holocene. Along the Mauritanian Margin, a step-like change in the transport of terrigenous material to the ocean that occurred at ~5.5 ka points to an abrupt transition between the African humid period and the more arid Late Holocene in the Western Sahara (deMenocal et al., 2000; Adkins et al., 2006). These observations suggest that positive feedbacks may have operated in the Western Sahara, e.g. vegetation changes may have triggered abrupt rainfall responses to gradual insolation forcing (Tjallingii et al., 2008; Claussen, 2009; Krinner et al., 2012). A recent dataset for water bodies from the Sahara and the Sahel regions supports humid conditions between ~15°N and 25°N during the mid-Holocene climate optimum (Lézine et al., 2011a).

African climate records located closer to the equator also demonstrate contrasting Holocene precipitation histories. For example, a sedimentary record from Lake Tanganyika in eastern equatorial Africa suggests an abrupt transition toward drier conditions during the mid-Holocene as compared to present-day (Tierney et al., 2008). In contrast, a progressive aridification

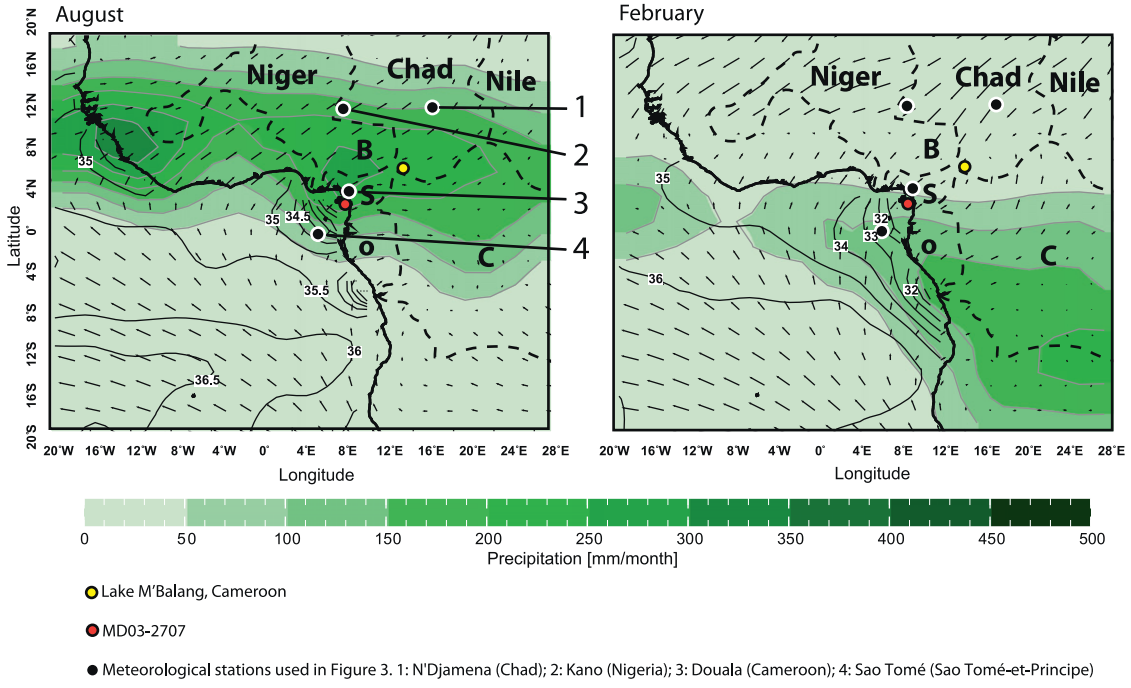

Fig. 1. Precipitation rates and surface wind fields over the Western equatorial Africa and Eastern equatorial Atlantic Ocean for August (left panel) and January (right panel). The red and yellow dots indicate sediment core location of MD03-2707 (this study) and Lake M'Balang (Vincens et al., 2010), respectively. Sea Surface Salinity is reported in the oceanic realm and derived from Antonov et al. (2010). The dashed lines on the continent outline the major river and paleo-river catchments (Niger, Chad, Nile, B=Benué, S=Sanaga, O=Ogooué, C=Congo). Wind data are derived from NCEP reanalysis (http://iri.ldeo.colombia.edu). (For interpretation of the references to colour in this figure legend, the reader is referred to the web version of this article.)

occurring within the Congo River catchment was recorded from a marine core collected close to the Congo River mouth (Schefuß et al., 2005). Multi-proxy salinity reconstructions from one marine sediment core situated in the eastern equatorial Atlantic indicates that the surface seawater was fresher during the mid-Holocene than today (Weldeab et al., 2007a). The paleosalinity records of this marine core capture rainfall changes integrated over river catchments situated mainly in the northern tropics.

A more careful evaluation of salinity reconstructions from the same sedimentary sequence, however, indicated divergent salinity trends for the late Holocene (Weldeab et al., 2007a). In particular, local salinity as estimated by Ba/Ca and $\delta^{18}O_{sw}$ suggests increasing and decreasing salinity trends during the late Holocene, respectively, implying that these reconstructions do not capture regional hydrological features in the same manner. Such observations, together with recent studies indicating that proxy specificities can induce contrasted trends in Holocene paleoclimate records (Leduc et al., 2010; Schneider et al., 2010) led us to reexamine salinity estimations from this region.

3. Modern climatology and its impact on the isotopic composition of seawater

3.1. Regional climatology and oceanography

The present-day rainfall patterns in western equatorial Africa are characterized by latitudinal shifts in precipitation maxima related to seasonal movements of the Intertropical Convergence Zone (ITCZ, Fig. 1). Seasonal maxima occur in northern tropical Africa during boreal summer and in southern tropical Africa during boreal winter. Those rainfall patterns alternately feed the Niger and Congo River drainages during boreal summer and winter seasons, respectively. These river drainage systems, which are channelled by the continental topography, are responsible for ocean salinity minima localized close to the Niger and Congo river mouths (Fig. 1).

The Gulf of Guinea surface hydrology is characterized by high sea surface temperature (SST) (>26 °C) and low salinity (<32) (Antonov et al., 2010). The surface currents of the eastern equatorial Atlantic, of which the major contributor is the Guinea Current, converge toward the Cameroon Margin (Gyory et al., 2005) and help sustain a low-salinity surface layer confined in the Gulf of Guinea (Figs. 1 and 2). Sediment core MD03-2707 (02°30.11′N, 09°23.68′E, 1295 m water depth) was collected in this low-salinity region (Figs. 1 and 2). While the present-day seasonal range of SST is small at the core location (varying between 26 °C in August and 28 °C in February), the sea surface salinity (SSS) experiences substantial seasonal fluctuations, reaching a maximum of ~33 during summer and a minimum of ~29 in winter (Antonov et al., 2010). The combination of high temperature and low salinity induces permanent surface ocean stratification, making the coring site a region with one of the strongest pycnoclines in the World Ocean, and preventing local upwelling from altering surface water characteristics (Fiedler and Talley, 2006).

3.2. Regional isotopic composition of seawater and rainfall

Because salinity and $\delta^{18}O_{sw}$ are both influenced by the balance between evaporation and precipitation in the open ocean, past changes in SSS are commonly reconstructed by estimating $\delta^{18}O_{sw}$ using planktonic foraminifera contained in marine sediments. On a global scale, there is a $\delta^{18}O_{sw}$ increase of ~0.5‰/salinity unit (Schmidt, 1999). At low latitudes, however, intense evaporation results in high $\delta^{18}O_{sw}$ values, so that the slope of the $\delta^{18}O_{sw}$/salinity relationship is less steep for tropical surface seawater than elsewhere. In the eastern equatorial Atlantic, comparison of SSS (Antonov et al., 2010) and modelled $\delta^{18}O_{sw}$ (LeGrande and Schmidt, 2006) indicate $\delta^{18}O_{sw}$/salinity varying between ~0.06 and 0.18‰/salinity unit, with the lowest slope localized near the Niger River Mouth (Fig. 2). These values agree well with the 0.08‰/salinity value established using core-top planktonic foraminifera from the eastern equatorial Atlantic (Fairbanks et al., 1992).

The computed $\delta^{18}O_{sw}$/salinity relationship shown in Fig. 2 is derived from the $1^\circ \times 1^\circ$ gridded $\delta^{18}O_{sw}$ database published by Schmidt et al. (1999). But poor data coverage in the eastern equatorial Atlantic (LeGrande and Schmidt, 2006) and the omission of some data points that were not representative of open-ocean conditions may bias the $\delta^{18}O_{sw}$/salinity relationship shown in Fig. 2 (LeGrande and Schmidt, 2006). However, these slopes (Fig. 2c), together with core-top analyses (Fairbanks et al., 1992), highlight that the $\delta^{18}O_{sw}$ in this region is not very sensitive to salinity, which may complicate paleosalinity reconstructions based on seawater isotopes (Fairbanks et al., 1992; Ravelo and Fairbanks, 1992).

To illustrate how the amount effect influences the regional isotopic composition of rainfall we analyze the relationship between the precipitation rates and the isotopic composition of rainwater across a series of meteorological stations located on a transect from the wet equatorial eastern Atlantic Ocean coast to the sub-arid western tropical Africa (Figs. 1 and 3). Monthly

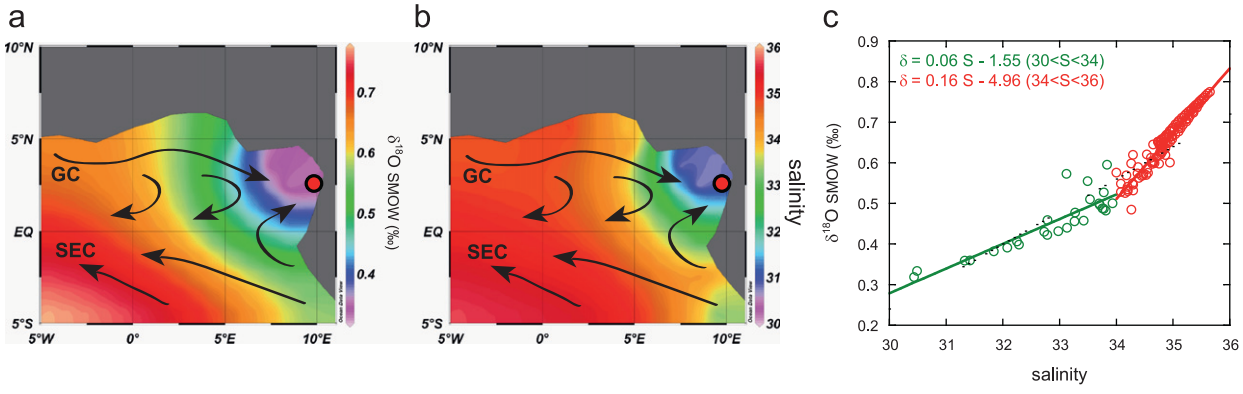

Fig. 2. (a) Mapping of eastern equatorial Atlantic $\delta^{18}O_{sw}$ (LeGrande and Schmidt, 2006); (b) Mapping of eastern equatorial Atlantic SSS (Antonov et al., 2010); (c) Regional linear relationship between $\delta^{18}O_{sw}$ and SSS extracted from the datasets shown in panels (a) and (b), with red and green colours corresponding to water salinity above and below 34, respectively. The red dot and arrows in panels (a) and (b) indicate MD03-2707 core location and major surface current flows in the region (Gyory et al., 2005), respectively. GC=Guinea Current, SEC=South Equatorial Current. (For interpretation of the references to colour in this figure legend, the reader is referred to the web version of this article.)

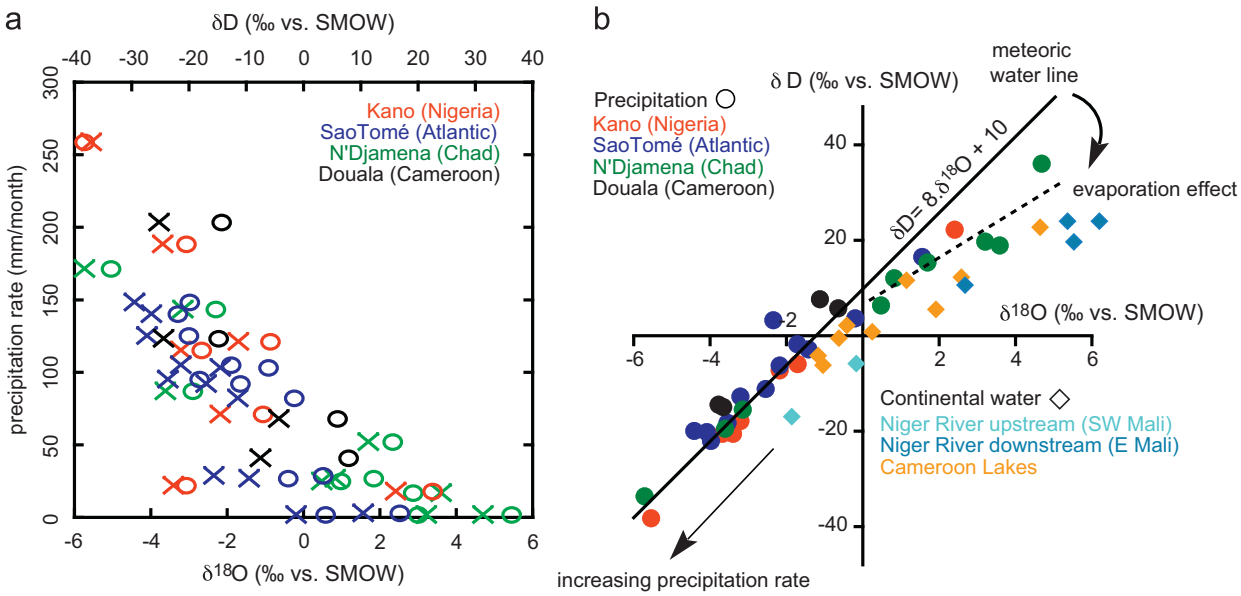

Fig. 3. (a) Modern-day monthly-based rainfall amount as a function of rainwater isotopic composition for four stations located in Fig. 1. Crosses are $\delta^{18}O$ values and circles are δD values. (b) $\delta^{18}O/\delta D$ relationships from the same dataset of rainfall (circles), as well as from continental freshwater available for Mali and Cameroon (GNIR data, Atlas of Isotope Hydrology—Africa, 2007). Also shown are the meteoric water line (Craig, 1961) and the effect of intense evaporation and resulting deviation from the meteoric water line. For better visualization, data with precipitation rates larger than 400 mm/months from the Douala station have been omitted since they exhibit consistently low isotopic ratios and are well aligned with the meteoric water line. (For interpretation of the references to colour in this figure legend, the reader is referred to the web version of this article.)

precipitation data from the region indicate that high precipitation rates are consistently related to lower hydrogen and oxygen isotopic values of rainfall, as expected from the amount effect (Craig, 1961; Risi et al., 2008; Fig. 3). Regional rainfall isotopic values are relatively heavy as compared to other monsoon regions where water vapour is transported over longer distances and experiences more isotopic distillation before precipitating (see e.g. Breitenbach et al., 2010). There are some months when significant amounts of precipitation are related to high isotopic values, i.e. $\delta^{18}O_r$ well above -2‰ when precipitation rates were higher than 100 mm/month (Fig. 3). In the sub-arid regions such as in Nigeria and Chad, $\delta^{18}O_r$ can exceed 2‰ during dry months (Fig. 3b). Such high isotopic values, together with a slight departure of $\delta^{18}O_r$ and rainfall δD (δD_r) from the meteoric water line (Fig. 3) suggest that the regional rainfall has experienced evaporation.

The evaporation occurring in northern tropical Africa in turn results in a progressive isotopic enrichment of environmental water. This is illustrated by the isotopic composition of Niger River water, which becomes increasingly enriched along its path (Fig. 3), and by the isotopic composition of lakes in Cameroon (Fig. 3). This process is analogous to that observed in rivers and lakes from east Africa (Craig and Gordon, 1965; Hillaire-Marcel and Casanova, 1987). Indeed, the same isotopic enrichment is observed in rivers and lakes from Chad, Niger and Nigeria (IAEA, 2007), suggesting that the freshwater ultimately reaching the Gulf of Guinea ought to be isotopically enriched compared to precipitation feeding the rivers. Keeping in mind the potential biases linked to the $\delta^{18}O_{sw}$/salinity relationship shown in Fig. 2, we extrapolate a freshwater $\delta^{18}O_{sw}$ end-member of -1.5‰ from the data located closest to the coast from the low-salinity regression ($\delta^{18}O_{sw} = 0.06 \times S - 1.55$). This value is somewhat higher than precipitation $\delta^{18}O$ values found in other equatorial regions, which are usually between about -3‰ and -6‰ (see e.g. Aggarwal et al., 2004; Benway and Mix, 2004; Schmidt et al., 2007). Evaporation of continental surface waters can at least partly explain the high freshwater end-member isotopic values in the $\delta^{18}O_{sw}$/salinity computation shown in Fig. 2.

4. Methods

The age model for the Holocene period is extensively described in Weldeab et al. (2007a) and is based on 12 radiocarbon measurements performed on planktonic foraminifera using a constant 400 yr reservoir age and the MARINE04 calibration curve (Hughen et al., 2004). Sediment samples for lipid analyses were taken from 2 to 5 cm thick sections which, according to the age model, represents ~100 yr per sample without accounting for bioturbation.

Lipids were extracted from ~10 g of freeze-dried sediments by pressurized fluid extraction (Dionex ASE-200) using a 9:1 (v/v) mixture of dichloromethane (DCM) and methanol. A lipid subfraction (compounds less polar than fatty acids) containing the long-chain alkenones of interest was isolated from the extracted lipids by solid-phase extraction on an aminopropyl column using a 3:1 (v/v) mixture of hexane and DCM.

The methyl $C_{37:2}$ ketones were purified from the lipid subfraction using high-performance liquid chromatography–mass spectrometry (HPLC–MS) following the procedure of Schwab and Sachs (2009), with minor modifications. This purification of the $C_{37:2}$ alkenone by HPLC–MS is required before compound-specific hydrogen isotope measurements by gas chromatography–isotope ratio mass spectrometry (GC–IRMS) due to inadequate baseline separation between the $C_{37:2}$ alkenones and $C_{37:3}$ alkenones and coeluting alkenoates. Such purification is crucial since co-occurring $C_{37:2}$ and $C_{37:3}$ can have δD values which are offset by as much as 45‰ (D'Andrea et al., 2007), implying that significant changes in the $U^{k'}_{37}$ index linked to changes in sea surface temperature can affect the δD_a records.

The HPLC–MS system consisted of an Agilent 1100 series high-performance liquid chromatograph equipped with a Prevail Cyano column (250 mm × 4.6 mm, 5 μm particle size; Alltech, Deerfield CA); fraction collector; and a quadrupole-based mass spectrometer. Sample injection volumes were typically 100 μl. Optimal compound separation was achieved using a mixture of 2.5% DCM (v/v) in hexane eluting at a flow rate of 1 mL/min and under isothermal conditions of 30 °C. This method resulted in $C_{37:2}$

alkenone retention times of ~30 min, with the $C_{37:3}$ alkenone eluting 2–3 min later and alkenoates eluting >10 min before $C_{37:2}$. Fraction collector vials containing the eluted $C_{37:2}$ fractions were appropriately combined, quantified, and evaluated for purity by gas chromatography–flame ionization detection (GC–FID) and gas chromatography–mass spectrometry (GC–MS) before GC–IRMS analyses. Quality control procedures included evaluating eluants immediately before and after the $C_{37:2}$ alkenone fractions to ensure complete compound recovery and, therefore, the isotopic integrity of the purified alkenones.

The stable hydrogen isotopic composition of $C_{37:2}$ was measured on a Thermo DELTA V GC–IRMS. Instrument performance and the $H3^+$ factor were monitored on a daily basis using a reference H_2 gas and a mixture of n-alkanes of known isotopic composition (Zhang and Sachs, 2007). Isotopic values were calculated with the ISODAT software using co-injection standards comprising C_{38} and C_{41} n-alkanes with known hydrogen isotopic composition bracketing the compound of interest. Small shoulder peaks were observed in some of the samples on the leading edge of the $C_{37:2}$ peaks during GC–IRMS runs, resulting in relatively large (~4‰) standard deviation. Because these shoulders were inconsistently integrated by the ISODAT software, all chromatograms were re-integrated manually to include the shoulder. This led to a reduction of the standard deviation of replicate analyses to <3‰. A subsequent manual integration that excluded the shoulder from the integrated peak resulted in identical downcore changes in the isotopic values on both the long-term and short-term timescales, indicating that the alkenone δD trends are insensitive to the integration technique. Excluding the shoulder, however, resulted in δD values that were systematically offset by −3‰, likely reflecting the fact that excluding the shoulder removes part of the alkenone peak that is enriched in deuterium (Schwab and Sachs, 2009). The δD_a values are based on the mean of three replicate analyses, and two samples containing abundant $C_{37:2}$ were reanalyzed from one day to another to monitor GC–IRMS drift over the measurement time period.

5. Results

The average temporal resolution of the δD record is better than 300 yr (Fig. 4). δD_a values were between −195‰ and −210‰, with highest values at ~3 ka and lowest values during the early Holocene and the core top (Fig. 4). A long-term increase from 10 to 3 ka was followed by a similar amplitude decrease in δD_a values over the last 3 ka. The standard deviation of δD_a measurements and the time resolution does not permit insight into hydrological changes at the submillennial timescale, so we exclusively focus on these long-term features.

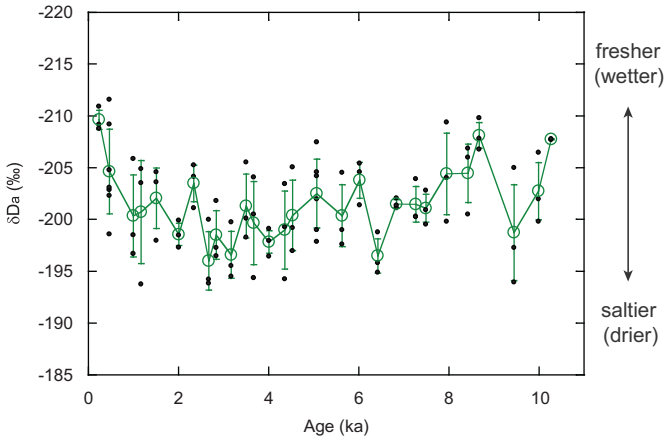

Fig. 4. Downcore changes in alkenone δD (δD_a). The black dots represent replicate measurements; the green circles and corresponding error bars represent their respective means and standard deviation. (For interpretation of the references to colour in this figure legend, the reader is referred to the web version of this article.)

5.1. Comparison of δD trends with those from other salinity proxies

Estimation of $\delta^{18}O_{sw}$ is routinely applied to infer past changes in the hydrological cycle in the tropics, based on the assumption that the modern-day $\delta^{18}O_{sw}$/salinity relationship has remained constant over time. This assumption has not been rigorously evaluated, and there is reason to expect it to be invalid under different climate boundary conditions. Modelling experiments of the Holocene climate have demonstrated that temporal changes in the slope of the $\delta^{18}O_{sw}$/salinity relationship coincide with regional hydrological changes, thus impacting salinity estimates independent of salinity changes (Schmidt et al., 2007; LeGrande and Schmidt, 2006). This effect is most pronounced at low latitudes, where the slope of the $\delta^{18}O_{sw}$/salinity relationship is relatively low (LeGrande and Schmidt, 2006).

We also use the Ba/Ca measured on planktonic foraminifera as a proxy for local input of freshwater. Because dissolved Ba is derived from weathering on land, dissolved Ba concentrations are highest in estuaries where Ba desorbs from suspended sediments. In large tropical estuaries such as those at the mouths of the Amazon, the Congo and the Ganges–Brahmaputra Rivers, Ba desorbs within the 0–6 salinity range; at higher salinity the behaviour of Ba is then conservative (see e.g. Edmond et al., 1978; Coffey et al., 1997 and references therein). At coastal sites that are heavily influenced by riverine runoff—such as in the Gulf of Guinea, Ba concentrations in seawater have a high inverse correlation with salinity (Weldeab et al., 2007a). Dissolved Ba is then incorporated into the calcium carbonate shells of planktonic foraminifera, which closely track seawater Ba concentrations (Lea and Spero, 1994). Thus foraminiferal Ba/Ca is a proxy for salinity that is independent of water isotopes and the hydrologic processes that affect them.

When δD_a are compared to the estimates of $\delta^{18}O_{sw}$ from Mg/Ca and $\delta^{18}O$ of planktonic foraminifera and to Ba/Ca-derived salinity estimates, each of the three salinity proxies displays a different Holocene trend (Fig. 5). In particular, the late Holocene δD_a and $\delta^{18}O_{sw}$ trends indicate decreasing isotopic values suggesting a decrease in salinity, while the Ba/Ca-derived salinity indicates increasing salinity trend.

$C_{37:2}$ alkenones are synthesized by certain species of coccolithophorids (in the ocean, mainly *Emiliania huxleyi* and *Geophyrocapsa oceanica*), while both $\delta^{18}O_{sw}$ and Ba/Ca are derived from planktonic foraminifera. Below we focus our discussion on the possible reasons for diverging trends between isotopic and Ba/Ca-derived salinity histories, while recognizing the possibility that seasonal production and vertical migrations of coccolithophorids and planktonic foraminifera could be an additional source of variation. To our knowledge, no studies have reported modern data for the season or depth habitats of planktonic organisms in the Gulf of Guinea so far. At low latitudes, *G. ruber* has been suggested to mainly thrive during the northern hemisphere summer season regardless of the hemisphere, as the Holocene SST trends estimated by Mg/Ca in MD03-2707 and elsewhere at equatorial latitudes tracks the northern hemisphere summer insolation (Leduc et al., 2010). Using an ecophysiological model of planktonic foraminifer growth and distribution, Lombard et al. (2011) simulated a maximum growth rate of *G. ruber* occurring in September. This coincides with the highest freshwater discharge of the Sanaga River, which increases from July to October along with concentrations of dissolved silica and chlorophyll a

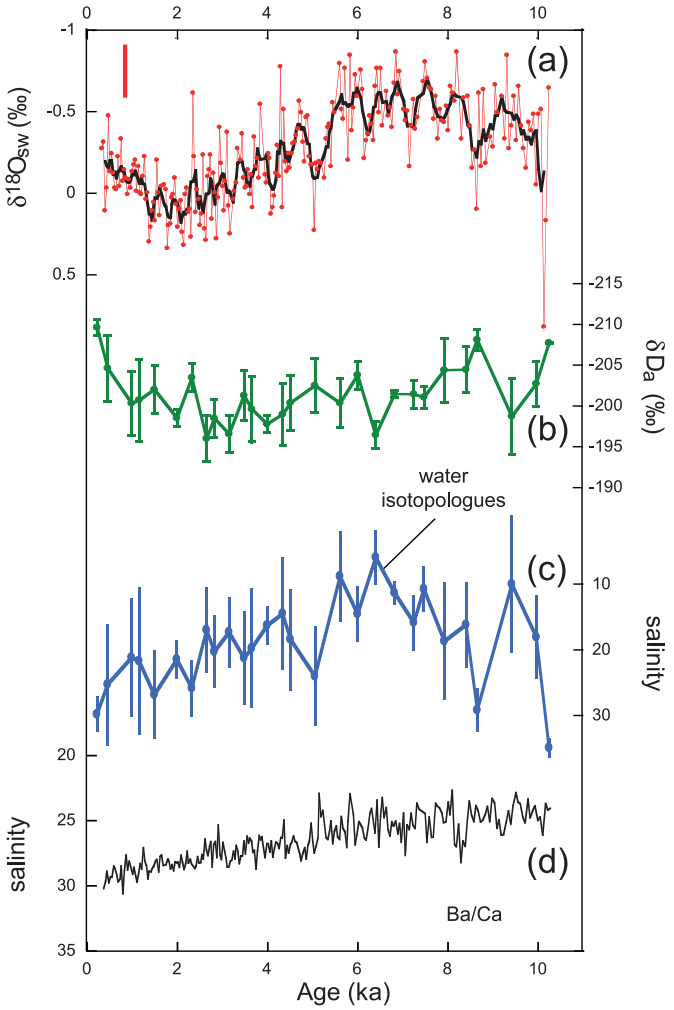

Fig. 5. Comparison of downcore changes in different salinity proxies measured on MD03-2707. (a) Downcore changes in $\delta^{18}O_{sw}$ (red dots are raw data from Weldeab et al. (2007a), black line is a 5-pt running average used in the computation of salinity shown in panel c); (b) downcore changes in δD_a (green curve, this study and simplified from Fig. 4); (c) salinity reconstruction based on water isotopologues (blue curve with dots, this study) using Eq. (1) from Rohling (2007) and its associated standard error (see text for details of calculation); (d) comparison of downcore salinity changes as estimated by Ba/Ca (thin black curve, Weldeab et al., 2007a). (For interpretation of the references to colour in this figure legend, the reader is referred to the web version of this article.)

(Weldeab et al., 2007c). If seasonal changes in chlorophyll-a can be used as a proxy for productivity of coccolithophorids, then foraminifera-based $\delta^{18}O_{sw}$ and Ba/Ca as well as alkenones may sample hydrological features occurring during maximum freshwater discharges at our coring site. Of course we cannot rule out the possibility that changes in the seasonality occurred in the past. Given the magnitude of salinity changes recorded by all the proxies shown in Fig. 5 and the divergent trends implied by both foraminifera-based salinity proxies, it seems unlikely that differences in the season and/or depth of alkenone and *G. ruber* production are primarily responsible for the first-order and long-term changes observed.

δD_a variations in the Holocene do not support a substantial increase in salinity over the last 10 ka, unlike that inferred from Ba/Ca in foraminifera (Fig. 5). Instead, δD_a suggest a slight salinity increase between 10 and 3 ka, followed by a salinity decrease over the last 3 ka. If the Ba/Ca-derived Holocene salinity increase of 6 salinity units is correct, it would be expected to cause a progressive increase in seawater δD of ~3‰ if both the modern $\delta^{18}O_{sw}$/salinity (Fig. 2) and $\delta^{18}O_{sw}/\delta D_{sw}$ (Rohling, 2007) relationships remained unchanged over the last 10 ka. An additional 6‰ increase in δD_a would be predicted to accompany a 6 salinity unit increase based on the ~1‰ decrease in hydrogen isotope fractionation expressed in algal and cyanobacterial lipids per unit increase in salinity observed in tropical evaporative ponds (Sachse and Sachs, 2008) and the mid-latitude Chesapeake Bay estuary (Sachs and Schwab, 2011). An even larger 18‰ increase in δD_a would be projected for the 6 unit salinity increase based on the culture experiments of Schouten et al. (2006), while little or no change in δD_a would be projected based on the trend of δD_a in the Chesapeake Bay (Schwab and Sachs, 2011).

At this stage it is worth noting that parameters other than δD_{sw} and salinity, such as growth rate (Schouten et al., 2006; Zhang et al., 2009) or growth stage (Volhowe et al., 2010), can impact δD_a. The influence of these parameters cannot be assessed in the present study; we assume here that they remained constant during the Holocene. While a 5–10‰ increase in δD_a recorded for the 10–3 ka time interval is consistent with $\delta^{18}O_{sw}$ data, the last 3 ka are marked by a 10‰ decrease, a trend that is consistent with reconstructed $\delta^{18}O_{sw}$ for the same time interval but not with the salinity trend from Ba/Ca (Fig. 5).

5.2. Salinity estimation using dual $\delta^{18}O_{sw}$ and δD_a

Rohling (2007) described a theoretical framework to reconstruct salinity by combining $\delta^{18}O_{sw}$ and δD_a. That method proposes to use differences in the way by which oxygen and hydrogen isotopes are fractionated slightly differently in the hydrological cycle to estimate changes in the freshwater flux and, by extension, salinity. The proposed estimate of salinity change is calculated as follows:

$$\Delta S = S_0\left(\frac{(\Delta\delta D_a/C)-\lambda\Delta\delta Ow}{\delta Dw_0-\lambda\delta Ow_0-d}\right) \quad (1)$$

where ΔS is the temporal salinity change induced by freshwater fluxes relative to the core top values, S_0 is the modern-day salinity (i.e. 30 at core location), $\Delta\delta D_a$ is the temporal change in the δD_a relative to the core top δD_a values, C is the constant that accounts for the fact that δD_a values change more rapidly than δD_{sw} because of salinity and growth rates (this constant is a factor to scale the δD_a to the δD_{sw} such that if the δD_{sw} is known then $C=1$; as developed below, growth rate cannot be determined and is here considered as constant), λ is the slope of the $\delta^{18}O/\delta D$ relationship of the meteoric water line (i.e. ~8 and considered as constant in space and time), $\Delta\delta O_{sw}$ is the temporal change in the $\delta^{18}O_{sw}$ relative to the core top $\delta^{18}O_{sw}$ values, δDw_0 and δOw_0 are the initial (i.e. modern-day as estimated at core top) seawater hydrogen and oxygen isotopic values, and d the deuterium excess of seawater (likely to be very close to 10 in open-ocean sites). As C, λ, d, δDw_0 and δOw_0 are considered constant through time, salinity changes are ultimately determined by the differences between temporal changes in $\delta D-\lambda\delta^{18}O$ weighted by the salinity effect on δD_a values.

A direct implication linked to the computation of salinity using the equation of Rohling (2007) is that the magnitude of salinity change will be determined by the constant C which accounts for parameters affecting hydrogen isotope fractionation such as salinity itself, growth rates of alkenone-synthesizing coccolithophorids, and other environmental parameters. In the batch culture experiments performed by Schouten et al. (2006), salinity and growth rates both impacted the D/H fractionation of alkenones. This led Rohling (2007) to use a value of 2.65 for the C constant in Eq. (1) which takes into account those two mechanisms, as Rohling was interested in reconstructing past changes in δD_{sw}. Since reconstructing past changes in coccolithophorid growth rates is currently not possible, they are assumed to have

been constant during the Holocene. In the culture experiment of Schouten et al. (2006), growth rates varied by a factor of 3 as salinity changed, which resulted in the observed $\delta D_a/\delta D_{sw}$ relationship of 2.65 ultimately used in Rohling (2007). Here we use a $\delta D_a/\delta D_{sw}$ relationship of 1.91 for the constant C, which is based on the salinity impact on hydrogen isotope fractionation as observed in the studies of Sachse and Sachs (2008) and of Sachs and Schwab (2011). These investigations reported a value for the D/H fractionation factor of lipids with respect to salinity closer to 1 (i.e. 1‰ increase in δD_a per salinity unit). Such a fractionation factor was observed to be remarkably constant over a large variety of other lipids previously collected in a large array of environmental settings (Sachs and Schwab, 2011), and is likely an accurate estimate of the salinity effect on hydrogen isotopes fractionation in lipids (Sachse et al., 2012). We acknowledge that a recent study (Schwab and Sachs, 2011) reported no influence of salinity on alkenone D/H fractionation over a salinity gradient ranging from 10 to 29 in the Chesapeake Bay estuary. The relevance of this finding to the present study is unclear. The assemblage of alkenone producers in an estuary is likely to be quite different than in the ocean, and the mechanisms by which euryhaline prymnesiophytes osmoregulate may influence the hydrogen isotopic signature of alkenones (Schwab and Sachs, 2011). We further note that using a value of 2.65 for the C constant would decrease the magnitude of the estimated salinity increase during the last 7 ka by ~40%, while a value of 1 (i.e. assuming no influence of salinity on D/H fractionation in alkenones) would increase the magnitude of the estimated salinity increase during the last 7 ka by ~50%. An additional limitation of Eq. (1) for estimating paleosalinity is that specifying a value for C implies *a priori* knowledge of salinity changes, as salinity itself is a significant factor affecting δD_a fractionation. Introducing the term C hence makes the salinity estimation non-linear, but the progressive increase in salinity over the last 7 ka remains a robust feature regardless the choice of C. Ideally, a proxy for past changes in δD_w would not be influenced by salinity, but we nevertheless demonstrate below that important insights into past climate regimes can be obtained from hydrogen isotopes in alkenones in the Gulf of Guinea.

To calculate salinity using the $\delta^{18}O_{sw}$ and δD_a records (Fig. 5c), we used the mean δD_a values (Fig. 5b) and the corresponding $\delta^{18}O_{sw}$ of the 5-point running average of the $\delta^{18}O_{sw}$ record (Fig. 5b). Such procedure acts to smooth the salinity record by removing significant point-to-point scattering apparent in the $\delta^{18}O_{sw}$ record (Fig. 5a). Part of the spread in the $\delta^{18}O_{sw}$ values probably results from centennial $\delta^{18}O_{sw}$ variability (Weldeab et al., 2007b), which is unlikely to be captured by alkenones because (1) alkenones are more prone to bioturbation than foraminifera, and (2) alkenones were extracted from thicker sedimentary intervals than those from which foraminifera were selected (up to 5 cm for alkenones vs. 1 cm slides for foraminifera) to ensure recovery of alkenones in sufficient quantities for δD analysis.

The errors associated with the terms used to compute salinity propagate are as follows:

$$\sigma_{\Delta S}^2 = \sum_{i=1}^{n} \left(\frac{\partial \Delta S}{\partial X_i}\right)^2 \sigma_{X_i}^2 \quad (2)$$

Rohling (2007) reported that the standard error was essentially linked to the errors associated with the terms $\Delta\delta D_a$ and $\Delta\delta O_{sw}$. We hence calculate the error propagation of salinity estimate following Rohling (2007) as follows:

$$\sigma_{\Delta S} = \sqrt{\left(\frac{\partial \Delta S}{\partial \Delta_{\delta Da}} \sigma_{\Delta \delta Da}\right)^2 + \left(\frac{\partial \Delta S}{\partial \Delta_{\delta O18w}} \sigma_{\delta O18w}\right)^2} \quad (3)$$

We use a constant value of 0.3 for $\sigma_{\delta O18w}$ and the resulting standard deviation calculated among δD_a measurements replicates for $\sigma_{\Delta\delta Da}$.

Using Eq. (1), the reconstructed salinity (Fig. 5c) based on paired foraminifera-derived $\delta^{18}O_{sw}$ and δD_a look nothing like the salinity trends inferred from $\delta^{18}O_{sw}$ or δD_a alone (Fig. 5a and b, respectively). In particular, the salinity trends derived from Eq. (1) imply an increase in salinity from the mid- to late Holocene opposite to that implied by the $\delta^{18}O_{sw}$ and δD_a alone (Fig. 5). It suggests that the modern water isotope/salinity relationship has changed through time, and that those changes have acted to reverse isotopic trends without any reversal in the salinity trend.

According to the propagation of error in the salinity estimation, the increase in salinity recorded between the mid-Holocene and the modern-day is significant (Fig. 5c). Salinity trends estimated for the last 3 ka, however, are only marginally significant, as standard errors associated with salinity estimations at ~3 ka and at core top overlap (Fig. 5c). Embedded within the long-term salinity increase during the last 7 ka is an abrupt increase at ~5.5 ka, coincident with the abrupt drying inferred from other records in Northwestern and Eastern equatorial Africa (deMenocal et al., 2000; Tierney et al., 2008). Overall, the salinity estimation based on derived water isotopologues appears to faithfully capture the Holocene aridification of northern tropical Africa.

When compared to the Ba/Ca-based salinity reconstruction, the new isotope-based salinity estimation implies large discrepancies in both the magnitude and the temporal trends of salinity (Fig. 5). For example, a decrease in salinity inferred from derived isotopologues occurred between ~10 and 6 ka, during which time the Ba/Ca-based salinity remained constant (Fig. 5). A t-test performed on the decreasing salinity trend recorded between 10 ka and 6 ka is statistically significant at the 95% confidence interval. It is unclear which process was responsible for this mismatch. Abrupt early Holocene changes in ice volume may have perturbed the oceanic budget of oxygen and hydrogen isotopes (Tjallingii et al., 2010), in a way that its net effect on the salinity calculation cannot be easily resolved given the uncertainties of the salinity influence on δD_a. Rising sea level during the early Holocene may also have caused desorption of Ba from sub-aerial sediments as the Niger and Sanaga River deltas were flooded, perturbing the Ba/Ca-salinity relationship in the Gulf of Guinea during this time interval.

Furthermore, the salinity values calculated using Eq. (1) are very low (~10–15) during the mid-Holocene (Fig. 5), implying values below the salinity tolerance of 20 for cultured *G. ruber pink* (Bijma et al., 1990), the foraminifer used to compute $\delta^{18}O_{sw}$ in MD03-2707. Yet diatom assemblages from a nearby core indicate high contributions of freshwater and brackish diatoms during the early and mid-Holocene (Crosta et al., 2011). Regardless of the absolute magnitude of the salinity changes calculated from Eq. (1), the apparent trends combined with the aforementioned ecological constraints suggest very low SSS at the location of MD03-2702 during the early and mid-Holocene. Reconciling the different magnitudes of salinity change inferred from Eq. (1) and from Ba/Ca is possible if changes in coccolithophorid growth rates occurred in response to insolation forcing, which would have the effect of changing the constant C in Eq. (1), or if changes in the Ba/Ca-salinity relationship occurred over time, perhaps as sub-aerial deltaic sediments were flooded as eustatic sea level rose in the early Holocene.

Over the last 3 ka, the geomorphology of the Niger and Sanaga River estuaries was probably much more stable than during the early Holocene. During this time interval, δD_a decreased by 10‰, reversing the increasing trend from 8 – 3 ka (Fig. 5), while the salinity trend based on foraminifera Ba/Ca implies an increase of

about 3 salinity units. If the increase in Ba/Ca-derived salinity 3–0 ka is correct, roughly 7‰ of the 10‰ decrease in δD_a can be ascribed to δD_{sw} changes if a 1‰ decrease in water–lipid D/H fractionation per unit increase in salinity is assumed (Sachse and Sachs, 2008; Sachs and Schwab, 2011). Over the same time interval, $\delta^{18}O_{sw}$ decreased by ~0.3‰ (Fig. 5). The $(\Delta\delta D_a/C) - 8\Delta\delta^{18}O_{sw}$ term from Eq. (1) which is ultimately used to derive salinity changes would then be lowered from ~7.6 to 4.6, implying that salinity changes derived from Eq. (1) may be overestimated when Ba/Ca is used as a diagnostic for changes in the impact of salinity on the δD_a. This bias may at least partly explain why the mid-Holocene salinity estimates using water isotopologues are much lower than those estimated from Ba/Ca in the studied region. Other processes causing water isotope fractionation in the atmosphere around Africa might also account for the over-estimation of the salinity change by the isotopologue approach. Noteworthy is the simulation by LeGrande and Schmidt (2011) in which the isotopologue-based salinity estimation technique provided much smaller errors than the traditional $\delta^{18}O_{sw}$ technique almost everywhere except in the Gulf of Guinea and the Mediterranean Sea, where a significant overestimation of salinity changes by the isotopologue technique occurred (LeGrande and Schmidt, 2011).

Even though the magnitude of Holocene salinity changes in the Gulf of Guinea may be overestimated by the isotopologue method described in Rohling (2007), the direction of the changes are consistent with most paleoclimate reconstructions from continental northern Africa. In particular, the salinity changes based on water isotopologues indicate a salinity increase over the last 6 ka, differing markedly from the salinity trends suggested by $\delta^{18}O_{sw}$ or δD_a values independently (Fig. 5). Changes in salinity resulting from the potential of variability in the constant C in Eq. (1) are considered to not have affected the computation of salinity trends at first order, especially over the last 3 ka when isotopic and non-isotopic proxies significantly diverge. We hence interpret the opposing trends in salinity using water isotopologues and both oxygen and hydrogen isotopes separately as indicative of changes in the seawater isotope/salinity slope through time.

6. Discussion

On time scales of 10^3 to 10^5 yr, the first-order driving mechanisms of rainfall changes in the northern tropics are changes in the Earth's orbit geometry. Summer insolation in the northern tropics

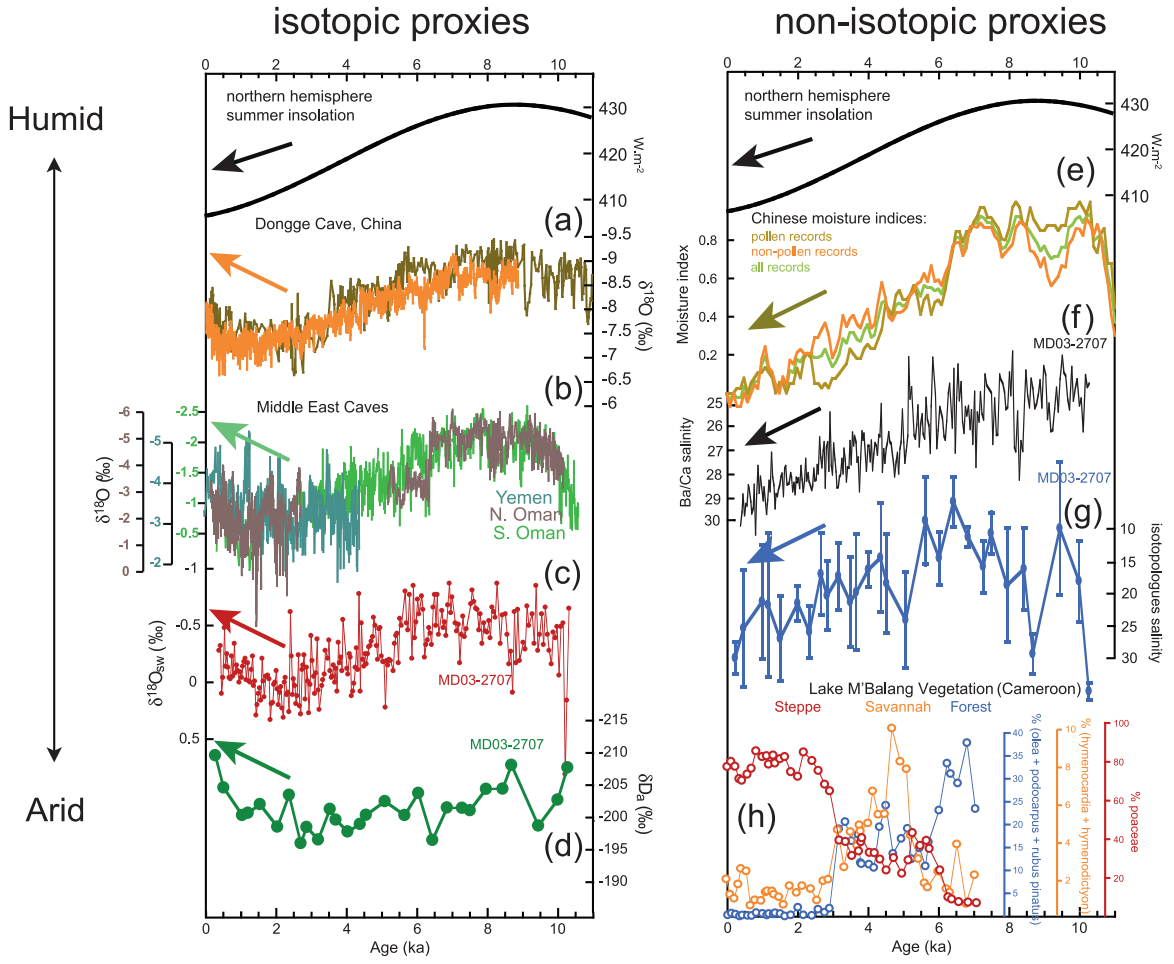

Fig. 6. MD03-2707 downcore changes in salinity proxies shown in Fig. 5 compared to other low-latitude precipitation proxies. Left panels indicate isotopic records and right panels indicate non-isotopic records; temporal changes in northern hemisphere summer insolation (Laskar, 1990) are reported on top of both panels. (a) Chinese speleothems $\delta^{18}O$ from Dongge Cave (purple curve, Dykoski et al., 2005; orange curve, Wang et al., 2005); (b) speleothems from Middle East caves (Fleitmann et al., 2003; Fleitmann et al., 2007); (c) $\delta^{18}O_{sw}$ changes in MD03-2707 (red dots, Weldeab et al., 2007a,b,c); (d) δD_a changes in MD03-2707 δD_a (green curve, this study); (e) moisture indices in China derived from a database containing a large array of proxies (green, orange and purple curves, Wang et al., 2010); (f) MD03-2707 salinity changes as estimated by Ba/Ca (thin black curve, Weldeab et al., 2007a,b,c); (g) MD03-2707 salinity changes as estimated by water isotopologues using Eq. (1) from Rohling (2007) (blue curve with dots, this study); (h) vegetation changes in Cameroon as estimated from Lake M'Balang (Vincens et al., 2010). Note that while the isotopic records indicate a trend reversal towards lighter isotopes over the last 3 ka, the non-isotopic records as well as the salinity estimate based on water isotopologues indicates a progressive aridification over the last 7 ka (see arrows). (For interpretation of the references to colour in this figure legend, the reader is referred to the web version of this article.)

decreased continuously over the entire Holocene, presumably causing the northern Africa dessication during the Holocene (see e.g. Lézine et al., 2011a and references therein). For example, the late Holocene was marked by the disappearance of the large endoreic Lake Mega-Chad which existed during the mid-Holocene and that drained into the Benué River catchment, the largest tributary to the Niger River (Sepulchre et al., 2008; Fig. 1). A multitude of other studies of sedimentary sequences that do not use hydrogen or oxygen isotopes as proxies for precipitation (see e.g. Gasse, 2000, and references therein; Lézine et al., 2011a) further support a humid northern tropical Africa during the mid-Holocene. A sedimentary sequence from Lake M'Balang in Central Cameroon, situated much closer to the Gulf of Guinea than the African sites mentioned above, provides a record of vegetation changes and further supports a progressive dessication linked to a continual decrease in precipitation (Vincens et al., 2010; Fig. 6h). These vegetation changes indicate that the long-term Holocene aridification trend did not only occur in the Sahara region, but also extended to sites situated much closer to the equator in western Africa. The salinity increase in the Gulf of Guinea derived from the Ba/Ca and from water isotopologues (Fig. 6g) supports the pollen data. If such a monotonic increase of salinity over the last 6 ka in the Gulf of Guinea is correct, then the decrease in $\delta^{18}O_{sw}$ and δD_a over the last 3 ka does not represent changes in salinity.

One straigthforward way to explain the decrease in δD_a and $\delta^{18}O_{sw}$ as salinity increased over the last 3 ka is to invoke changes in the salinity/seawater isotope relationships. The surface seawater isotopic composition in the Gulf of Guinea is strongly affected by rivers draining northern tropical Africa. $\delta^{18}O_r$ and δD_r changes over land may have caused changes in the isotopic composition of the freshwater end members, in turn altering surface seawater isotopes at the location of MD03-2707. If the salinity trend reconstructed by Ba/Ca is assumed correct, it can be used to diagnose the impact of a changing freshwater end-member $\delta^{18}O$ on the salinity derived from $\delta^{18}O_{sw}$ alone, assuming the modern $\delta^{18}O_{sw}$/salinity relationship was constant through time. This is highlighted in Fig. 7. In this conceptual model, changes in the slope of the $\delta^{18}O_{sw}$/salinity relationship cause $\delta^{18}O_{sw}$ to increase between ~6 ka and 3 ka and then decrease from ~3 ka towards present-day $\delta^{18}O_{sw}$ values (Fig. 7). The postulated change in the slope of $\delta^{18}O_{sw}$/salinity from 6 to 3 ka and then from 3 to the present day would suggest $\delta^{18}O_{sw}$ to be a poor proxy for salinity. Its reversal ~3 ka does not reflect a change in hydrography in the Gulf of Guinea, but rather a change in the end member $\delta^{18}O_r$. The isotopic composition of this freshwater end-member is given in the equations reported in Fig. 7 for salinity values of zero, and suggests that the freshwater $\delta^{18}O$ values inherited from that of regional rainfall reached a maximum at around 3 ka. We urge caution in interpreting the freshwater end member values. The subsurface end member $\delta^{18}O$ value might have shifted over time, and the Ba/Ca-derived salinity values remain an estimation based on the modern seawater Ba/salinity relationship, which may also change with time. Past changes in the $\delta^{18}O_{sw}$/salinity suggested by Fig. 7 however highlight the possibility that the $\delta^{18}O_{sw}$/salinity slope was extremely shallow at ~3 ka, when the $\delta^{18}O_r$ may have been close to $\delta^{18}O_{sw}$. It yet appears likely that the opposite signs of $\delta^{18}O_{sw}$ trends recorded between 6 and 3 ka and between 3 and present-day were modulated by changes in the $\delta^{18}O_{sw}$/salinity, even as salinity increased continuously over this time period.

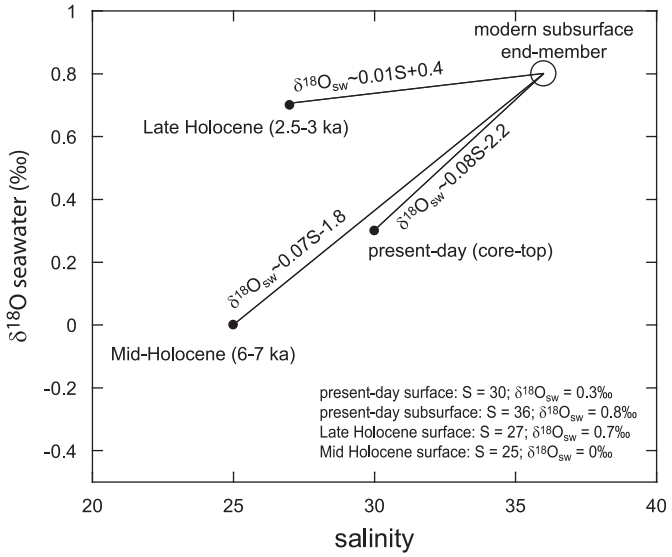

Fig. 7. Theoretical model illustrating the $\delta^{18}O_{sw}$/salinity relationship using the $\delta^{18}O_{sw}$ and Ba/Ca-derived data from Weldeab et al. (2007a,b,c) for the present-day, the 2.5–3 ka, and 6–7 ka time intervals. A hypothesized constant high-salinity end member computed using subsurface $\delta^{18}O_{sw}$ and salinity values is presented to illustrate how the $\delta^{18}O_{sw}$/salinity may have evolved over time. A +0.6‰ was added to the calculated $\delta^{18}O_{sw}$ to account for *G. ruber pink* vital effect (Deuser and Ross, 1989).

The salinity increase which occurred over the last 3 ka was probably associated with a decrease in the $\delta^{18}O$ of the freshwater end member and likely reflected changes in the regional $\delta^{18}O_r$. Despite the large uncertainties associated with the freshwater $\delta^{18}O$ as extrapolated in Fig. 7, it is useful to consider other archival sources for paleorecords of $\delta^{18}O_r$. Unfortunately estimates of $\delta^{18}O_r$ from lake sediments in northern tropical Africa are characterized by large dating uncertainties, low time resolution and sedimentary discontinuities, making it difficult to evaluate the Holocene $\delta^{18}O_r$ evolution in that area (Gasse, 2002). There are no speleothem records available from northwestern tropical Africa to monitor Holocene changes in $\delta^{18}O_r$. However speleothems from the northern Arabian Sea and southern Oman shed light on $\delta^{18}O_r$ in the eastern part of northern tropical Africa and the Middle East (Fleitmann et al., 2007 and references therein). When speleothems from Qunf Cave (Fleitmann et al., 2003), Hoti Cave and Dimarshim Cave (Fleitmann et al., 2007) are combined, they indicate that Holocene rainfall isotopic values probably reached a maximum ~2 ka (Fig. 6b). One such speleothem, the one collected in northern Oman, suggests $\delta^{18}O_r$ shifts comparable to the end-member values extrapolated from the $\delta^{18}O_{sw}$/salinity relationship in Fig. 7 over the last 3 ka. This implies that our conceptual model attempting to reconstruct past changes in the $\delta^{18}O_{sw}$/salinity relationship in the Gulf of Guinea in Fig. 7 captures plausible values for freshwater (rainfall) isotopic end-members, and adds confidence to the interpretation of Holocene salinity trends as estimated from water isotopologues. Interestingly, Chinese speleothems (Fig. 6a) share with Qunf Cave a late Holocene decrease in isotopic values that reverses the long-term increase between 7 and 3 ka, a feature similarly recorded in MD03-2707 $\delta^{18}O_{sw}$ and δD_a (Fig. 6c and d). We however note that neither the values nor the magnitude of $\delta^{18}O$ compares with those observed in the Middle East or with the extrapolated freshwater end-member in the Gulf of Guinea. This mismatch probably reflects the contrasting environmental settings between East Asia and northern tropical Africa, and in particular the long-distance transport of moisture which decreases the $\delta^{18}O_r$ recorded in Chinese speleothems. We also note that an extensive compilation of various proxy records of moisture from East Asia derived from a large array of proxies reveal a continuous aridification in China over the last 7 ka which contrasts with the speleothem records (Fig. 6e).

Transient model simulations further support a long-term aridification of the northern tropics in response to orbital forcing

(Fisher and Jungclaus, 2010). Taken at face value, a reversal in the trend of monsoon strength during the Late Holocene would go against current understanding of how the monsoon is expected to respond to orbital forcing. Modeling experiments that incorporate the water isotopes into atmosphere–ocean general circulation models may provide quantitative estimates of changes in rainfall isotopes together with precipitation rate variability. They indicate that the Holocene isotopic records of rainfall in tropical areas are strongly affected by water vapour transport, so that changes in the rainfall isotopic composition likely reflect regional atmospheric circulation changes rather than local precipitation changes (LeGrande and Schmidt, 2009; Hu et al., 2008; Dayem et al., 2010; Lewis et al., 2010; Pausata et al., 2011; Maher and Thompson, 2012).

Yet it remains to be determined what triggered the isotopic shifts in the freshwater end-member of Gulf of Guinea surface water. One potential process involves moisture recycling from vegetation in northern Africa. $\delta^{18}O_r$ from African meteorological stations indicate an overall increase in isotopic values from the maritime station of Sao Tomé to the sub-desert station of N'Djamena, southern Chad (Figs. 1 and 3). Sonntag et al. (1979) suggested that the Congo Basin rainforest is an important source of moisture for the regions situated to the north of the basin, a process expected to have repercussions on $\delta^{18}O_r$ and δD_r in those regions. As moisture released by transpiration is not affected by isotopic fractionation, the moisture derived from transpiration occurring on land will be isotopically enriched compared to water vapour with a marine origin. This would cause $\delta^{18}O_r$ (and δD_r) values of rainfall condensing from continental vapour isotopically enriched compared to rainfall condensing from vapour with a marine origin (see e.g. discussion in Rozanski et al. (1993)). During the early and mid-Holocene, when forests were more extensive in northern Africa, such an effect may have been more pronounced than it is today. The culmination of the African Humid Period over the last 6 kyr, with its associated diminution of forest cover, would have reduced this effect as the flux of transpired water from vegetation in northern Africa diminished, causing $\delta^{18}O_r$ to decline to today's lower values. Another potential process involves changes in the isotopic composition of precipitation along with convective activity (Risi et al., 2008). Modern observations indicate that extreme shifts in $\delta^{18}O_r$—varying by $\sim$5‰ from the convective zone to the stratiform zone—occur during the passage of squall lines over the Sahel region (Risi et al., 2008; Risi et al., 2010). Changes in regional monsoon flow over the Holocene may have changed the patterns of convective activity along squall lines (see e.g. Lézine et al., 2011b), modifying the $\delta^{18}O_r$ along storm tracks and above the drainage basins within which different types of convective activity occurred. Whether or not one of these two processes affected the $\delta^{18}O_r$ during the Holocene requires further investigation.

7. Conclusions

In this study we measured δD values of $C_{37:2}$ alkenones from a marine sedimentary sequence collected in the Gulf of Guinea spanning the last 10 ka. When compared to previously published reconstructions of salinity based on Ba/Ca and $\delta^{18}O_{sw}$, each shows a different trend through the Holocene. By using water isotopologues to infer past changes in salinity, we show that some of those discrepancies can be reconciled.

Our results illustrate for the first time how changes in the hydrological cycle can modulate changes in the seawater isotopes/salinity relationship and drive changes in $\delta^{18}O_{sw}$ without accompanying salinity changes. The most likely explanation for this disconnect are atmospheric processes that triggered changes in rainfall isotopic ratios over time in the Niger River basin. Similar changes in rainfall $\delta^{18}O$ are recorded in tropical speleothems from the Middle East and East Asia which support this hypothesis.

Acknowledgements

G.L. acknowledges financial support from the INTERDYNAMIK program as well as Alyssa Atwood, Maxime Bridoux, Ines Mügler and Dan Nelson for technical support. This material is based upon work supported by the US National Science Foundation under Grant no. 0639640 (J.P.S.). We thank two anonymous reviewers and Associate Editor J. Lynch-Stieglitz for their constructive comments that materially improved the manuscript.

References

Adkins, J.F., deMenocal, P.D., Eshel, G., 2006. The "African Humid Period" and the record of marine Upwelling from excess ^{230}Th in ODP hole 658C. Paleoceanography 21, PA4203, http://dx.doi.org/10.1029/2005PA001200.

Aggarwal, P.K., Fröhlich, K., Kulkarni, K.M., Gourcy, L.L., 2004. Stable isotope evidence for moisture sources in the Asian summer monsoon under present and past climate regimes. Geophys. Res. Lett. 31, L08203, http://dx.doi.org/10.1029/2004GL019911.

Alexandre, A., Meunier, J.-D., Lézine, A.-M., Vincens, A., Schwartz, D., 1998. Grassland dynamics in intertropical Africa during the late Holocene: a phytolith analysis. Palaeogeogr. Palaeoclimatol. Palaeoecol. 136, 213–229.

Antonov, J.I., Seidov, D.T., Boyer, P., Locarnini, R.A., Mishonov, A.V., Garcia, H.E., Baranova, O.K., Zweng, M.M., Johnson, D.R., 2010. World Ocean Atlas 2009, vol. 2. Levitus, S. (Ed.), NOAA Atlas NESDIS 69, US Government Printing Office, Washington, DC, 184 pp.

Benway, H., Mix, A., 2004. Oxygen isotopes, upper-ocean salinity, and precipitation sources in the eastern tropical Pacific. Earth Planet. Sci. Lett. 224, 493–507.

Bijma, J., Faber, W., Hemleben, C., 1990. Temperature and salinity limits for growth and survival of some planktonic foraminifers in laboratory cultures. J. Foraminiferal Res. 20, 95–116.

Breitenbach, S.F.M., Adkins, J.F., Meyer, H., Marwan, N., Kumar, K.K., Haug, G.H., 2010. Strong Influence of water vapor source dynamics on stable isotopes in precipitation observed in Southern Meghalaya, NE India. Earth Planet. Sci. Lett. 292, 212–220.

Coffey, M., Dehairs, F., Collette, O., Luther, G., Church, T., Jickells, T., 1997. The behaviour of dissolved barium in estuaries. Estuarine Coastal Shelf Sci. 45, 113–121.

Craig, H., 1961. Isotopic variations in meteoric waters. Science 133, 1702–1703.

Craig, H., Gordon, L.I., 1965. Deuterium and oxygen 18 variations in the ocean and marine atmosphere. In: Proceedings of Stable Isotopes in Oceanographic Studies and Paleotemperatures, 1965, Spoleto, Italy. Tongiogi, E. (Ed.), V. Lishi e F., Pisa, pp. 9–130.

Claussen, M., 2009. Late Quaternary vegetation-climate feedbacks. Clim. Past 5, 203–216.

Crosta, X., Romero, O.E., Ther, O., Schneider, R.R., 2011. Climatically-controlled siliceous productivity in the eastern Gulf of Guinea during the last 40,000 yr. Clim. Past Discuss. 7, 2445–2476.

D'Andrea, W.J., Liu, Z.H., Alexandre, M.D., Wattley, S., Herbert, T.D., Huang, Y., 2007. An efficient method for isolating individual long-chain alkenones for compound-specific hydrogen isotope analysis. Anal. Chem. 79, 3430–3435.

Dansgaard, W., 1964. Stable isotopes in precipitation. Tellus 16, 436–467.

Dayem, K.E., Molnar, P., Battisti, D.S., Roe, G.H., 2010. Lessons learned from oxygen isotopes in modern precipitation applied to interpretation of speleothem records of paleoclimate from eastern Asia. Earth Planet. Sci. Lett. 295, 219–230.

deMenocal, P.B., Ortiz, J., Guilderson, T., Sarnthein, M., 2000. Coherent high- and low-latitude climate variability during the Holocene warm period. Science 288, 2198–2202.

Deuser, W.G., Ross, E.H., 1989. Seasonally abundant planktonic-foraminifera of the Sargasso Sea: succession, deep-water fluxes, isotopic compositions, and paleoceanographic implications. J. Foraminiferal Res. 19, 268–293 1989.

Dykoski, C.A., Edwards, R.L., Cheng, H., Yuan, D., Cai, Y., Zhang, M., Lin, Y., Qing, J., An, Z., Revenaugh, J., 2005. A high-resolution, absolute-dated Holocene and deglacial Asian monsoon record from Dongge Cave, China. Earth Planet. Sci. Lett. 233, 71–86.

Edmond, J.M., Boyle, E.D., Drummond, D., Grant, B., Mislick, T., 1978. Desorption of barium in the plume of the Zaire (Congo) river. Neth. J. Sea Res. 12 (3–4), 324–328.

Englebrecht, A., Sachs, J., 2005. Determination of sediment provenance at drift sites using hydrogen isotopes and unsaturation ratios in alkenones. Geochimica et Cosmochimica Acta 69, 4253–4265.

Fairbanks, R.G., Charles, C.D., Wright, J.D., 1992. Origin of global meltwater pulses. In: Taylor, R.E. (Ed.), Radiocarbon after Four Decades. Springer-Verlag, pp. 473–500.

Fiedler, P.C., Talley, L.D., 2006. Hydrography of the eastern tropical Pacific: a review. Prog. Oceanogr. 69, 143–180.
Fisher, N., Jungclaus, J.H., 2010. Effects of orbital forcing on atmosphere and ocean heat transports in Holocene and Eemian climate simulations with a comprehensive Earth system model. Clim. Past 6, 151–168.
Fleitmann, D., Burns, S.J., Mudelsee, M., Neff, U., Kramers, J.D., Mangini, A., Matter, A., 2003. Holocene forcing of the Indian monsoon recorded in a stalagmite from Southern Oman. Science 300, 1737–1739.
Fleitmann, D., Burns, S.J., Mangini, A., Mudelsee, M., Kramers, J., Villa, I., Neff, U., Al-Subbary, A.A., Buettner, A., Hippler, D., Matter, A., 2007. Holocene ITCZ and Indian monsoon dynamics recorded in stalagmites from Oman and Yemen (Socotra). Quat. Sci. Rev. 26, 170–188.
Gasse, F., 2000. Hydrological changes in the African tropics since the Last Glacial Maximum. Quat. Sci. Rev. 19, 189–211.
Gasse, F., 2002. Diatom-inferred salinity and carbonate oxygen isotopes in Holocene waterbodies of the western Sahara and Sahel (Africa). Quat. Sci. Rev. 21, 737–767.
Gyory, J., B. Bischof, A.J. Mariano, E.H., Ryan, 2005. "The Guinea Current". Ocean Surface Currents. 〈http://oceancurrents.rsmas.miami.edu/atlantic/guinea.html〉.
Hillaire-Marcel, C., Casanova, J., 1987. Isotopic hydrology and paleohydrology of the Magadi (Kenya)–Natron (Tanzania) Basin during the laste Quaternary. Paleogeogr. Paleoclimat. Paleoecol. 58, 155–181.
Hu, C., Henderson, G.M., Huang, J., Xie, S., Sun, Y., Johnson, K.R., 2008. Quantification of Holocene Asian monsoon rainfall from spatially separated cave records. Earth Planet. Sci. Lett. 266, 221–232.
Hughen, K.A., Baillie, M.G.L., Bard, E., Beck, A.J.W., Bertrand, C.J.H., Blackwell, P.G., Buck, C.E., Burr, G.S., Cutler, K.B., Damon, P.E., Edwards, R.L., Fairbanks, R.G., Friedrich, M., Guilderson, T.P., Kromer, B., McCormac, G., Manning, S., Bronk Ramsey, C., Reimer, P.J., Reimer, R.W., Remmele, S., Southon, J.R., Stuiver, M., Talamo, S., Taylor, F.W., van der Plicht, J., Weyhenmeyer, C.E., 2004. MARINE04 marine Radiocarbon age calibration 26 – 0 ka BP. Radiocarbon 46, 1059–1086.
IAEA, 2007. Atlas of isotope hydrology—Africa. International Atomic Energy Agency reports, Vienna.
Krinner, G., Lézine, A.-M., Braconnot, P., Sepulchre, P., Ramstein, G., Grenier, C., Gouttevin, I., 2012. A reassessment of lake and wetland feedbacks on the North African Holocene climate. Geophys. Res. Lett. 39, L07701, http://dx.doi.org/10.1029/2012GL050992.
Kröpelin, S., Verschuren, D., Lézine, A.M., Eggermont, H., Cocquyt, C., Francus, P., Cazet, J.P., Fagot, M., Rumes, B., Russell, J.M., Darius, F., Conley, D.J., Schuster, M., von Suchodoletz, H., Engstrom, D.R., 2008. Climate-driven ecosystem succession in the Sahara: the past 6000 years. Science 320, 765–768.
Laskar, J., 1990. The chaotic motion of the solar system: a numerical estimate of the size of the chaotic zones. Icarus 88, 266–291.
Lea, D.W., Spero, H.J., 1994. Assessing the reliability of paleochemical tracers: barium uptake in the shells of planktonic foraminifera. Paleoceanography 9 (3), 445–452, http://dx.doi.org/10.1029/94PA00151.
Leduc, G., Vidal, L., Tachikawa, K., Bard, E., 2009. ITCZ rather than ENSO signature for abrupt climate changes across the tropical Pacific? Quat. Res. 72, 123–131.
Leduc, G., Schneider, R.R., Kim, J.-H., Lohmann, G., 2010. Holocene and Eemian sea surface temperature trends as revealed by alkenone and Mg/Ca paleothermometry. Quat. Sci. Rev. 29, 989–1004.
LeGrande, A.N., Schmidt, G.A., 2006. Global gridded data set of the oxygen isotopic composition in seawater. Geophys. Res. Lett. 33, L12604, http://dx.doi.org/10.1029/2006GL026011.
LeGrande, A.N., Schmidt, G.A., 2009. Sources of Holocene variability of oxygen isotopes in paleoclimate archives. Clim. Past 5, 441–455.
LeGrande, A.N., Schmidt, G.A., 2011. Water isotopologues as a quantitative paleosalinity proxy. Paleoceanography 26, PA3225, http://dx.doi.org/10.1029/2010PA002043.
Lewis, S.C., LeGrande, A.N., Kelley, M., Schmidt, G.A., 2010. Water vapour source impacts on oxygen isotope variability in tropical precipitation during Heinrich events. Clim. Past 6, 325–343.
Lézine, A.M., Hely, C., Grenier, C., Braconnot, P., Krinner, G., 2011a. Sahara and Sahel vulnerability to climate changes, lessons from Holocene hydrological data. Quat. Sci. Rev. 30, 3001–3012.
Lézine, A.M., Zheng, W., Braconnot, P., Krinner, G., 2011b. Late Holocene plant and climate evolution at Lake Yoa, northern Chad: pollen data and climate simulations. Clim. Past 7, 1351–1362.
Lombard, F., Labeyrie, L., Michel, E., Bopp, L., Cortijo, E., Retailleau, S., Howa, H., Jorissen, F., 2011. Modelling planktonic foraminifer growth and distribution using an ecophysiological multi-species. Biogeosciences 8, 853–873.
Maher, B., Thompson, R., 2012. Oxygen isotopes from Chinese caves: records not of monsoon rainfall but of circulation regime. J. Quat. Sci. 27, 615–624.
Marriner, N., Flaux, C., Kaniewski, D., Morhange, C., Leduc, G., Moron, V., Chen, Z., Gasse, F., Empereur, J.-Y., Stanley, J.-D., 2012. ITCZ and ENSO-like pacing of Nile delta hydro-geomorphology during the Holocene. Quat. Sci. Rev. 45, 73–84.
Pahnke, K., Sachs, J.P., Keigwin, L.D., Timmermann, A., Xie, S.-P., 2007. Eastern tropical Pacific hydrologic changes during the past 27,000 years from D/H ratios in alkenones. Paleoceanography 22, PA4214, http://dx.doi.org/10.1029/2007PA001468.
Pausata, F.S.R., Battisti, D.S., Nisancioglu, K.H., Bitz, C.M., 2011. Chinese stalagmite δ^{18}O controlled by changes in the Indian monsoon during a simulated Heinrich event. Nat. Geosci. 4, 474–480.
Ravelo, A.C., Fairbanks, R.G., 1992. Oxygen isotopic composition of multiple species of planktonic foraminifera: recorders of the modern photic zone temperature gradient. Paleoceanography 7, 815–832.
Risi, C., Bony, S., Vimeux, F., Descroix, L., Ibrahim, B., Lebreton, E., Mamadou, I., Sultan, B., 2008. What controls the isotopic composition of the African monsoon precipitation? Insights from event-based precipitation collected during the 2006 AMMA field campaign. Geophys. Res. Lett. 35, L24808, http://dx.doi.org/10.1029/2008GL035920.
Risi, C., Bony, S., Vimeux, F., Chong, M., Descroix, L., 2010. Evolution of the water stable isotopic composition of the rain sampled along Sahelian squall lines. Q. J. R. Meteorol. Soc. 136, 227–242.
Rohling, E.J., 2007. Progress in palaeosalinity: overview and presentation of a new approach. Paleoceanography 22, PA3215, http://dx.doi.org/10.1029/2007PA001437.
Rozanski, K., Araguas-Araguas, L., Gonfiantini, R., 1993. Isotopic patterns in modern global precipitation. In: Climate Change in Continental Isotope Records, AGU Monograph 78, pp. 1–36 (1993).
Sachs, J.P., Schwab, V., 2011. Hydrogen isotopes in dinosterol from the Chesapeake Bay estuary. Geochim. Cosmochim. Acta 75, 444–459.
Sachse, D., Sachs, J.P., 2008. Inverse relationship between D/H fractionation in cyanobacterial lipids and salinity in Christmas Island saline ponds. Geochim. Cosmochim. Acta 72, 793–806.
Sachse, D., Billault, I., Bowen, G.J., Chikaraishi, Y., Dawson, T.E., Feakins, S.J., Freeman, K.H., Magill, C.R., McInerney, F.A., van der Meer, M.T.J., Polissar, P., Robins, R., Sachs, J.P., Schmidt, H.-L., Sessions, A.L., White, J.W.C., West, J.B., Kahmen, A., 2012. Molecular paleohydrology: interpreting the hydrogen-isotopic composition of lipid biomarkers from photosynthesizing organisms. Annu. Rev. Earth Planet. Sci. 40, 221–249.
Schefuß, E., Schouten, S., Schneider, R.R., 2005. Climatic controls on central African hydrology during the past 20,000 years. Nature 437, 1003–1006.
Schmidt, G.A., 1999. Error analysis of paleosalinity calculations. Paleoceanography 14, 422–429, http://dx.doi.org/10.1029/1999PA900008.
Schmidt, G.A., G.R., Bigg, E.J., Rohling, 1999. Global Seawater Oxygen-18 Database—v1.21. 〈http://data.giss.nasa.gov/o18data/〉.
Schmidt, G.A., LeGrande, A.N., Hoffmann, G., 2007. Water isotope expressions of intrinsic and forced variability in a coupled ocean-atmosphere model. J. Geophys. Res. 112, D10103, http://dx.doi.org/10.1029/2006JD007781.
Schneider, B., Leduc, G., Park, W., 2010. Disentangling seasonal signals in Holocene climate trends by satellite-model-proxy integration. Paleoceanography 25, PA4217, http://dx.doi.org/10.1029/2009PA001893.
Schouten, S., Ossebaar, J., Schreiber, K., Kienhuis, M.V.M, Langer, G., Benthien, A., Bijma, J., 2006. The effect of temperature, salinity and growth rate on the stable hydrogen isotopic composition of long chain alkenones produced by *Emiliania huxleyi* and *Gephyrocapsa oceanica*. Biogeosciences (3), 113–119.
Schwab, V.F., Sachs, J.P., 2009. The measurement of D/H ratios in alkenones and their isotopic heterogeneity. Org. Geochem. 40, 111–118.
Schwab, V., Sachs, J.P., 2011. Hydrogen isotope in alkenones from the Chesapeake Bay Estuary. Geochim. Cosmochim. Acta 75, 7552–7565.
Sepulchre, P., Schuster, M., Ramstein, G., Krinner, G., Girard, J.-F., Vignaud, P., Brunet, M., 2008. Evolution of Lake Chad Basin hydrology during the mid-Holocene: a preliminary approach from lake to climate modelling. Global Planet. Change 61, 41–48.
Sonntag, C., Klitzsch, E., Löhnert, E.P., El-Shazly, E.M., Münnich, K.O., Junghans, Ch., Thorweihe, U., Weistroffer, K., Swailem, F.M., 1979. Paleoclimatic information from deuterium and oxygen-18 in carbon-14 dated north Saharian groundwaters. In: Isotope Hydrology 1978, vol. II. International Atomic Energy Agency, Vienna, pp. 569–581.
Tierney, J.E., Russell, J.M., Huang, Y., Sinninghe Damsté, J.S., Hopmans, E.C., Cohen, A.S., 2008. Northern Hemisphere controls on tropical southeast African climate during the past 60,000 years. Science 322, 252–255.
Tjallingii, R., Stattegger, K., Wetzel, A., Van Phach, P., 2010. Infilling and flooding of the Mekong River incised valley during deglacial sea-level rise. Quat. Sci. Rev. 29, 1432–1444.
Tjallingii, R., Claussen, M., Stuut, J.-B., Fohlmeister, J., Jahn, A., Bickert, T., Lamy, F., Röhl, U., 2008. Coherent high- and low-latitude forcing of the Northwest African humidity. Nat. Geosci. 1, 670–675.
Van der Meer, M.T.J., Sangiorgi, F., Baas, M., Brinkhuis, H., Sinninghe Damsté, J.S., Schouten, S., 2008. Molecular isotopic and dinoflagellate evidence for Late Holocene freshening of the Black Sea. Earth Planet. Sci. Lett. 267, 426–434.
Van der Meer, M.T.J., Baas, M., Rijpstra, W.I.C., Marino, G., Rohling, E.J., Sinninghe Damsté, J.S., Schouten, S., 2007. Hydrogen isotopic compositions of long-chain alkenones record freshwater flooding of the Eastern Mediterranean at the onset of sapropel deposition. Earth Planet. Sci. Lett. 262, 594–600.
Vincens, A., Buchet, G., Servant, M., ECOFIT Mbalang collaborators, 2010. Vegetation response to the "African Humid Period" termination in Central Cameroon (7°N)—new pollen insight from Lake Mbalang. Clim. Past 6, 281–294.
Volhowe, M.D., Prahl, F.G., Probert, I., Maldonado, M., 2010. Growth phase dependent hydrogen isotopic fractionation in alkenone-producing haptophytes. Biogeosciences 6, 1681–1694.
Wang, Y.J., Cheng, H., Edwards, R.L., He, Y.Q., Kong, X.G., An, Z.S., Wu, J.Y., Kelly, M.J., Dykoski, C.A., Li, X.D., 2005. The Holocene Asian monsoon: links to solar changes and North Atlantic climate. Science 308, 854–857.
Wang, Y., Liu, X., Herzschuh, U., 2010. Asynchronous evolution of the Indian and East Asian Summer Monsoon indicated by Holocene moisture patterns in monsoonal central Asia. Earth-Sci. Rev. 103, 135–153.
Weldeab, S., Lea., D.W., Schneider, R.R., Andersen, N., 2007a. 155,000 years of West African monsoon and ocean thermal evolution. Science 316, 1303–1307.

Weldeab, S., Lea., D.W., Schneider, R.R., Andersen, N., 2007b. Centennial scale climate instabilities in a wet early Holocene West African monsoon. Geophys. Res. Lett. 34, L24702, http://dx.doi.org/10.1029/2007GL031898.

Weldeab, S., Schneider, R.R., Müller, P., 2007c. Comparison of Mg/Ca- and alkenone-based sea surface temperature estimates in the fresh water-influenced Gulf of Guinea, eastern equatorial Atlantic. Geochem. Geophys. Geosyst. 8, Q05P22, http://dx.doi.org/10.1029/2006GC001360.

Zhang, Z., Sachs, J.P., 2007. Hydrogen isotope fractionation in freshwater algae: I. Variations among lipids and species. Org. Geochem. 38, 582–608.

Zhang, Z., Sachs, J.P., Marchetti, A., 2009. Hydrogen isotope fractionation in freshwater and marine algae: II. Temperature and nitrogen-limited-growth-rate effects. Org. Geochem. 40, 428–439.